Available online at www.sciencedirect.com
SCIENCE DIRECT®
International Journal of Solids and Structures 42 (2005) 1209–1224
INTERNATIONAL JOURNAL OF SOLIDS and STRUCTURES
www.elsevier.com/locate/ijsolstr

Modeling of perforation of plates and multi-layered metallic targets

Predrag Elek *, Slobodan Jaramaz, Dejan Micković

Faculty of Mechanical Engineering, University of Belgrade, 27. marta 80, 11120 Belgrade, Serbia and Montenegro

Received 10 December 2003; received in revised form 22 June 2004
Available online 23 August 2004

Abstract

The perforation of monolithic and multi-layered thin metallic plates by flat-ended cylindrical penetrator is considered. The most relevant analytical penetration models with their most important assumptions, basic process mechanisms, and key analytical relations for plugging mode of monolithic plates penetration are reviewed. Comparative analysis of computational results and our experimental data show significant compatibility of process basic parameters and also indicates certain limitations of the analytical models. It has been concluded that phenomenological model with deformable penetrator represents the best analytical approximation of penetration process. By modification of this model, the improved penetration model is created, whose results better correspond with experimental data. The improved model is applied to the analysis of perforation of multi-layered targets with spaced layers. Theoretical results for the case of double-layer target are especially analyzed. These results enable the formulation of certain conclusions of considerable practical importance.

Keywords: Perforation; Plugging; Analytical model; Multi-layered target; Ballistic limit velocity; Experimental investigation

1. Introduction

The paper considers the perforation of thin monolithic and multi-layered plates by cylindrical flat-ended penetrators—fragment simulators. In the case of normal impact, this penetrator/target combination is characterized by the plugging mode of perforation. The plugging usually occurs during the interaction of HE projectile fragment and different light-armored targets, so its investigation is important from the angle of projectile efficiency as well as from the point of target vulnerability. As a "compromise" between

* Corresponding author. Tel.: +381 113370383; fax: +381 113370364.
E-mail address: pelek@mas.bg.ac.yu (P. Elek).

0020-7683/$ - see front matter © 2004 Elsevier Ltd. All rights reserved.
doi:10.1016/j.ijsolstr.2004.06.053

empirical and numerical models, the analytical approach is chosen, which clearly shows the physics of process and enables efficient parametric studies. First, different analytical models are considered in the light of their accordance with our experimental results.

2. Analytical models of penetration

In the concise presentation of the most relevant multi-stage analytical penetration models, the normal impact at velocity v_0 of cylindrical flat-ended penetrator of mass m and diameter $2R$ into homogenous, plane metallic plate of thickness H and density ρ is assumed.

2.1. Energy-deformation model

This relatively simple penetration model by Woodward and de Morton (1976) is based on the application of two fundamental principles: (a) the law of propagation of deformation in target material, and (b) the law of energy conservation for the penetrator/target system. The motion and deformation of the cylindrical region of the target (primary zone) has been considered. This zone is located directly in front of the rigid projectile, while the remainder of target (secondary zone) is regarded as immovable. Immediately after the penetrator impact, the compression of primary zone starts by the mechanism of compressive wave propagation. From the momentum law, the velocity of the deformed region of the target v as a function of the strain ε is:

$$v = \frac{K\sigma_y}{\rho c_e} + \frac{2}{n+1}\sqrt{\frac{K\sigma_0 n}{\rho}}\left[\varepsilon^{\frac{n+1}{2}} - \left(\frac{K\sigma_y}{E}\right)^{\frac{n+1}{2}}\right], \tag{1}$$

where σ_y is the yield stress, E is the Young's modulus, c_e is the velocity of elastic disturbances in target material, $K > 1$ is the parameter of constrained deformation due to increase of plastic stress caused by the presence of surrounding target material that restrains the plug compression. Parameters σ_0 and n are constants in the constitutive equation $\sigma = \sigma_0 \varepsilon^n$.

The parameters of penetrator and plug motion are shown in Fig. 1. The assumptions of uniformly accelerated motion of the front part and decelerated motion of the back part of the plug, enable the determination of displacements L_F and L_B at time t.

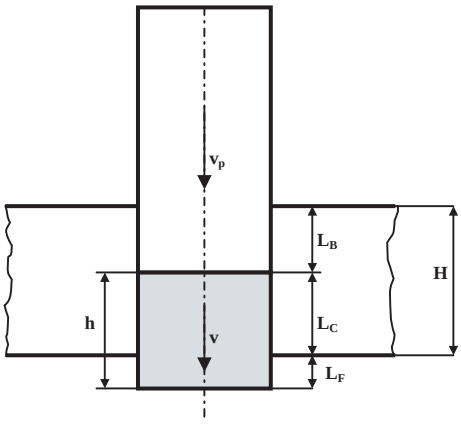

Fig. 1. Basic parameters of penetrator/target system by energy-deformation model.

The penetrator velocity can be determined by the energy conservation law in the form:

$$\frac{1}{2}mv_0^2 - \frac{1}{2}mv_p^2 = \sum_i W_i = W_C + W_K + W_S + W_F, \tag{2}$$

where v_p is penetrator velocity and W_i are penetrator works against compressive, inertial, shear and friction forces, which can be easily derived.

The previous analysis is related to the first, main stage of the penetration process. This phase can be finished in two ways: (a) by perforation—that completes the whole process—if the condition $L_B = H$ is fulfilled, or (b) by realization of the condition $v_p = v$, before (a), which leads to the second stage of the process.

The analysis of the second phase is quite simple, because the penetrator and the plug behave as a single body whose velocity can be determined from the energy conservation law (2) with omitted compressive work.

2.2. Structural model

The structural model developed by Woodward (1987) considers stresses and strains that lead to the plug formation, as well as the resistance of the whole structure. The process can be analyzed through two stages (Fig. 2). In the first stage, the penetrator and the region of target material that forms the plug are moving with common velocity v_p. Shearing of the plug also occurs with decreasing of the contact length h. The shear forces cause bending of the surrounding target material of a cylindrical shape, with increase of the external radius. When the increasing plug velocity v reaches penetrator velocity v_p, shear stops and the second phase commences, where besides bending, the extension of the secondary target zone dominates.

On the basis of the momentum and angular momentum laws, velocity of the penetrator together with the plug v_p, velocity v of the deformed part of the target and its dimension z in the first stage of penetration can be determined from the system of equations

$$\begin{aligned} &mv_0 - \left(m + \frac{1}{2}m_0R^2\right)v_p = \int_0^t Q_p\,dt, \quad \frac{1}{2}m_0vz\left(R + \frac{1}{3}z\right) = \int_0^t Q_p\,dt \\ &\frac{1}{3}m_0vz^2\left(R + \frac{1}{4}z\right) = -\int_0^t (M_{p0} + M_{pz})\,dt + \int_0^t Q_p z\,dt \end{aligned} \tag{3}$$

with loads (shear force and bending moments) defined by expressions

$$Q_p = \frac{2\pi}{\sqrt{3}}\sigma_y Rh, \quad M_{p0} = \frac{\pi}{2}\sigma_y Rh^2, \quad M_{pz} = \frac{\pi}{2}\sigma_y (R+z)H^2. \tag{4}$$

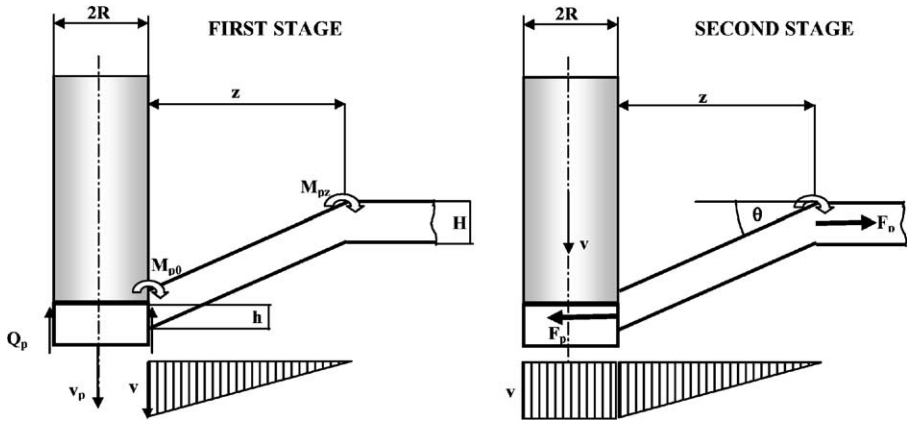

Fig. 2. Parameters of system in both stages of structural model.

In the second stage of penetration the same laws can be applied with modification of bending moments and introduction of extension forces. The perforation occurs when strain of the target material, caused by extension reaches the critical value. The whole process can be completed in one of the three possible ways: (a) by target perforation in the first stage owing to plastic shear along the whole thickness of the target, (b) by perforation in the second phase due to a fracture caused by extension, or (c) by arrestment of the penetrator due to insufficient impact velocity either in the first or in the second phase.

2.3. Three-stage model

A well-known Awerbuch and Bodner model of penetration (1974a, 1974b), whose main characteristic is that in the case of perforation the process always passes through three different stages, is based on the application of the law of motion of a variable mass body. The model requires experimental determination of three important parameters of the process: (a) entrance and exit (or average) diameter D of a cavity in the target after perforation, (b) plug length b, and (c) shear zone width e (radial dimension of deformed segment of the secondary target zone). The stages of penetration process are shown in Fig. 3.

The fundamental penetration mechanism is gradual addition of the target material to the penetrator, whose initial mass is m_0. The coordinate x, defining the penetration depth, is determined by the position of the front part of a new-added mass of the plug. The plug and the penetrator constitute the effective mass. The equation of motion of the effective mass is:

$$\frac{\mathrm{d}}{\mathrm{d}t}(mv) = -(F_i + F_C + F_S). \tag{5}$$

In the first stage the shear force F_S does not act, and the inertial force is determined by $F_i = k\rho A v^2/2$, where k is a factor depending on the penetrator nose shape. The compressive force is $F_C = \sigma_C A$, with σ_C as the ultimate compressive strength of the target material. The differential equation (5) yields the expression for the moving mass velocity during the first stage

$$v = \left[\left(\frac{m_0}{m_0 + \rho A x}\right)^{2+k}\left(v_0^2 + \sigma_C/\rho\left(1 + \frac{k}{2}\right)\right) - \sigma_C/\rho\left(1 + \frac{k}{2}\right)\right]^{\frac{1}{2}}. \tag{6}$$

The first stage ends when the condition $x = H - b$ is accomplished. At this moment shear forces start to act and the law of motion is changed.

In the second stage the equation of effective mass motion has a modified form (with the shear force $F_S = \pi D\tau(x - H + b)$, where $\tau = \tau_0 + \mu\dot{\gamma}$, $\dot{\gamma} = v/e$), which can be solved numerically. In the previous relations, τ_0 is a quasi-static ultimate shear strength, μ is a viscosity coefficient and γ is a shear angle. The second stage is ended as soon as $x = H$; at that moment, the plug is formed and its extrusion starts.

The third stage considers the body of constant mass $m = m_0 + \rho A h$, whose motion is resisted by shear force only, and the equation of motion can be simply solved. The third stage terminates with the plug

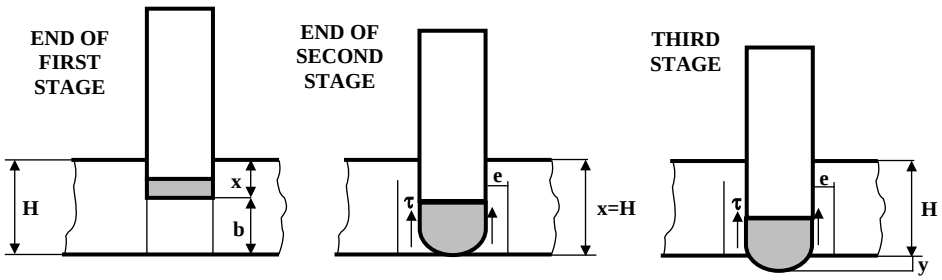

Fig. 3. Scheme of penetration stages in three-stage model.

ejection when the shear strain reaches its maximum value γ_f for the target material. Of course, the process can be finalized in other way—by the arrestment of the penetrator in the target, $v = 0$, in any stage.

2.4. Phenomenological model

This theoretical approach by Liss et al. (1983) considers the motion of both primary and secondary target zone and introduces very complex penetration mechanisms. Basically, it is a multi-stage model where compression and shear of the target material have a key role. Due to impulsive nature of the process, it is regarded that these stresses have a wave form.

Normal and shear stresses σ and τ in the target material under impulsive loading are defined by constitutive equations

$$\sigma = \frac{1}{1-\varepsilon}[\sigma_y - B\ln(1-\varepsilon)], \quad \tau = \tau_y + \frac{1}{3}B\gamma, \tag{7}$$

where B is a coefficient of the target material strengthen, σ_y and τ_y are quasi-static normal and shear yield stresses, ε and γ are engineering strain and shear angle. The real increased value of normal stress due to constrained deformation of the target material is determined by equation $\sigma_C = K\sigma$. Because of velocity and deformation discontinuity in the compression zone and undeformed zone, the propagation of compression wave is modeled by a shock wave concept. The typical configuration of deformation zones as well as geometry of the penetrator/target system is shown in Fig. 4a. The application of the momentum law and the relation between displacement and strain gives the following equations

$$c_p = \frac{v_1 - v_4}{\varepsilon} + v_4, \quad \varepsilon(\sigma_c - \sigma_{yc}) = \rho(v_1 - v_4)^2 \tag{8}$$

which enable the determination of unknown strain ε, velocity of plastic shock wave c_p and stresses σ and σ_c. In the phenomenological penetration model, the first stage lasts from the initial contact to the moment when zones 3 and 4 start to move with different velocities. The equations of motion in the first stage are:

$$\begin{aligned} \dot{v}_1 &= -\frac{\sigma_c A + \rho A(v_1 - v_4)^2 + 2\pi R\tau_q(x_2 - x_1)}{m + \rho A(x_2 - x_1)}, \quad v_1 = v_2, \\ \dot{v}_4 &= \frac{\rho A(v_1 - v_4)^2 + 2\pi R\tau_q(x_2 - x_1) - 2\pi rH(\tau_y + \rho c_s v_3)}{\rho\pi r^2 H - \rho A(x_2 - x_1)}, \quad v_3 = v_4 \end{aligned} \tag{9}$$

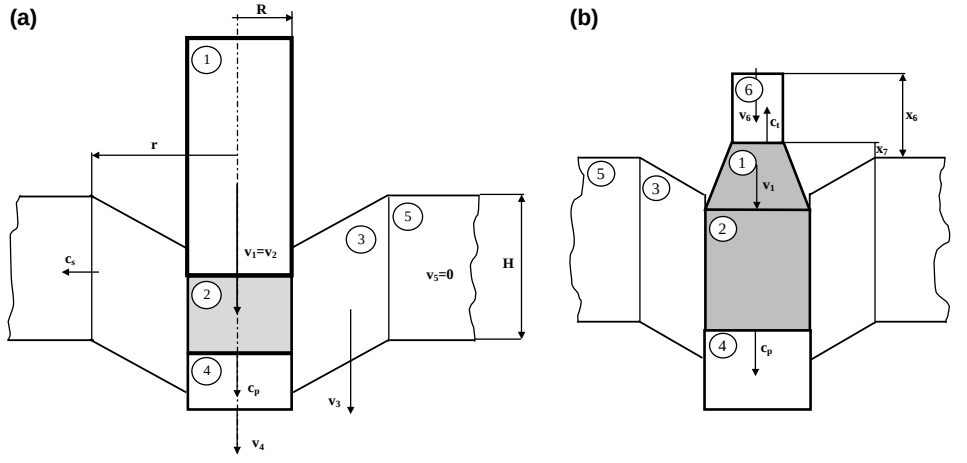

Fig. 4. Geometric configuration of penetrator/target system for (a) rigid and (b) deformable penetrator for phenomenological model.

where m, A and R are the penetrator mass, cross-section area and radius, H is target thickness, r and c_s are position and velocity of plastic hinge, τ_q is dynamic shear stress defined by (7), and v_i denotes velocity of ith zone.

In the second phase of penetration there are no new physical processes that would essentially change the equations of motion. This phase terminates with the arrestment of compression shock wave ($v_1 = v_4$), and the penetrator and the plug start to move as a single body.

In the final phase of penetration there is only shear force, so the process can be simply modeled. The perforation is completed when the plastic fracture occurs, i.e. when the condition $x_1 = x_3 + H$ is fulfilled.

It should be emphasized that more complicated "scenarios" of the process can exist, which are similarly modeled and which are in detail operated in the computer program.

The previous analysis implies undeformable penetrator; however, it is possible to generalize the model for the case of deformable penetrator (dp) (Liss and Goldsmith, 1984). If the constitutive equation (7) is also valid for a penetrator material, then by applying of the momentum law to the target and penetrator parts subjected to the deformation at the moment of initial contact, it can be derived that the real, reduced initial velocity of penetration is:

$$v' = \frac{v_0}{1+\sqrt{q}}, \quad q = \frac{\rho(\sigma_y + B)}{\rho_p(\sigma_{yp} + B_p)}, \tag{10}$$

where q is the parameter dependent on target and penetrator (subscript p) material characteristics. The typical configuration of zones during penetration by a deformable penetrator is given in Fig. 4b. The new zone 6 is represented by the undeformed portion of penetrator and defined by the plastic compressive shock wave position in the penetrator (with velocity c_t). Equations of motion, conditions for stages termination and phases of a penetration process are determined analogously to the model with rigid penetrator.

Each of the presented models is a good analytical solution for a certain class of metallic plates penetration problems. The survey of the analyzed models applicability is presented in Table 1. The computer programs, developed for every model, give an expectedly good reproduction of the literature results. For drawing the complete conclusions, a comparison with a new experimental data is doubtlessly useful.

3. Comparison of experimental and computed results

The scheme of experimental devices and measuring equipment for investigation of penetration is shown in Fig. 5 (Jaramaz and Micković, 2000).

The standard steel penetrator for perforation of steel plates with lower and higher thickness (1.25 and 2.2 mm) has been used with different impact velocities (400–950 m/s). The basic properties of penetrator and plates are given in Table 2.

The measured parameters of the process relevant for comparison with the computed results are: (a) residual penetrator velocity measured by make-up screens and relative deformation of penetrator diameter due to compression, (b) plug length and (c) plate deflection (maximum displacement of the secondary target zone after perforation).

The experimental values of mentioned parameters and results obtained by computer programs based on different analytical models are shown in Figs. 6–9. It should be mentioned that experimental results represent, in fact, average values of several measurements performed under "identical" conditions.

The residual velocity of penetrator as a function of its impact velocity is shown in Fig. 6. This dependance is fundamental and the most important indicator of models' validity. For the target with lower thickness (1.25 mm), it can be noticed that all analytical models give the acceptable evaluations of exit velocity (Fig. 6a). The experimental results are bounded by computed results of the structural (upper bound) and

Table 1
The applicability of the analyzed models according to the assumptions and experimental verifications

Theoretical model	Projectile	Target			Impact conditions
		Material	Material behavior	Thickness	
Energy-deformation model	• Rigid • Flat-ended	Steel, aluminum	Elastic–plastic	Thin, medium	• Normal impact • Single plate • V_0 up to 800 m/s
Structural model	• Rigid • Flat-ended	Mild steel, stainless steel, aluminum	Rigid-plastic	Thin	• Normal impact • Single plate • V_0 up to 300 m/s
Three-stage model	• Rigid • Deformable nose • Different nose shapes	Pure aluminum, Al alloy, mild steel, steel alloy	Rigid-plastic	Thin, medium	• Normal impact • Single plate • $V_0 = 400$, 850 m/s
Phenomenological model	• Rigid • Flat-ended	Aluminum, steel	Rigid-plastic	Thin, medium	• Normal impact • Single plate • V_0 up to 1000 m/s
Phenomenological model (dp)	• Rigid/deformable • Flat-ended	Aluminum	Rigid-plastic	Thin, medium	• Normal impact • Single plate • V_0 up to 600 m/s

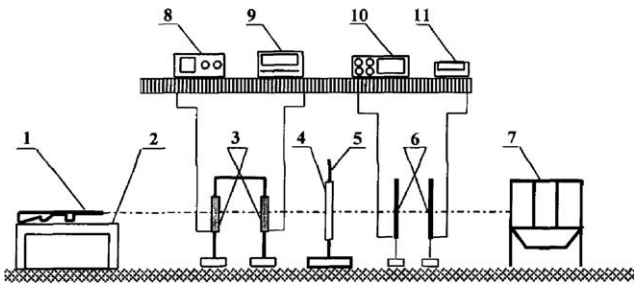

Fig. 5. Scheme of experiment and specification of measuring equipment. 1—Automatic rifle ARMALITE AR-18, 5.56 × 45 mm, 2—universal stand, 3—lumiline screens, 4—plate, 5—supporting frame, 6—make-up screens, 7—catching box, 8—counter, 9—amplifier, 10—universal counter and 11—transmitter unit.

the energy-deformation model (lower bound). The other three models produce very low discrepancy from measured values. Having in mind that the three-stage model uses certain experimentally determined parameters, it can be regarded that the phenomenological model with a deformable penetrator is the most effective analytical tool. This was expected considering the model complexity. However, for the target of higher thickness (2.2 mm, Fig. 6b), the situation is substantially different—all models yield unsatisfactory results. The reasons for significant deviations of computed results, especially in the domain of low residual velocities, are primarily in the fact that the plate of higher thickness is in the zone between the thin targets and targets with medium thickness, where different penetration models are valid. Therefore, the considered

Table 2
Basic characteristics of penetrator and plates used in the experiment

Penetrator		Plate	
Material	Steel	Material	Steel
Hardness (HB)	243	Hardness (HB)	80
Mass (g)	1.411	Normal yield stress (MPa)	320
Maximum diameter (mm)	5.71	Transversal dimensions (mm)	400 × 400

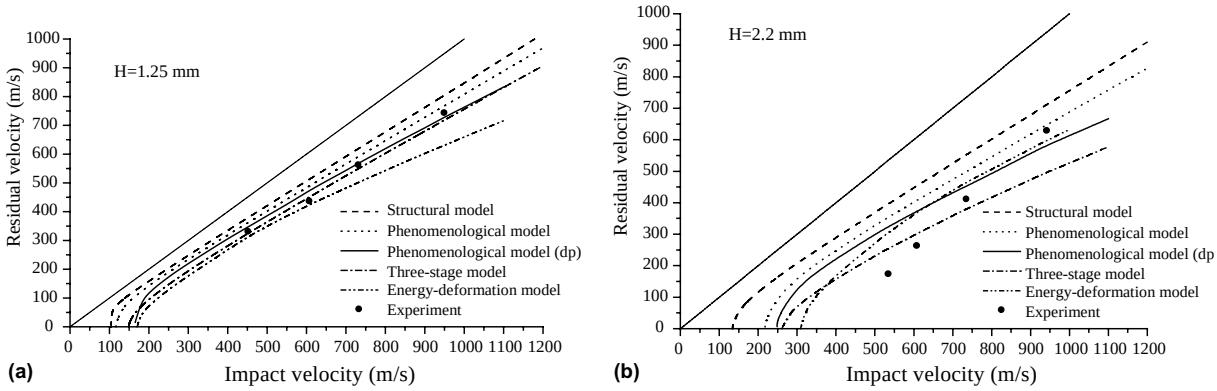

Fig. 6. Penetrator residual velocity vs. impact velocity for the plate with (a) lower and (b) higher thickness.

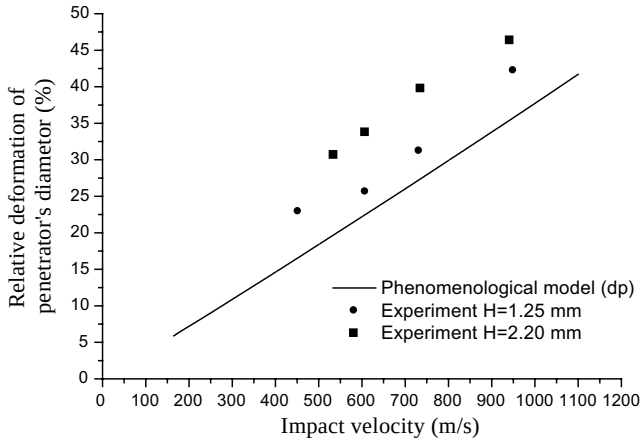

Fig. 7. Relative deformation of penetrator diameter vs. impact velocity.

analytical models provide very good evaluations of exit velocity, but only up to a certain limit of plate thickness.

The relative increase of penetrator diameter as a function of its impact velocity is shown in Fig. 7. The only model that does not assume a rigid striker is the phenomenological model with a deformable penetrator.

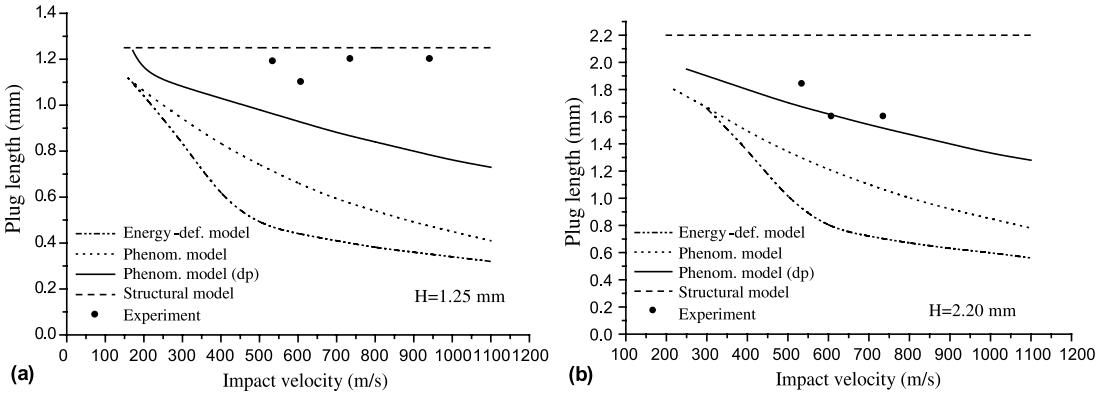

Fig. 8. Plug length as a function of impact velocity for the plate with (a) lower and (b) higher thickness.

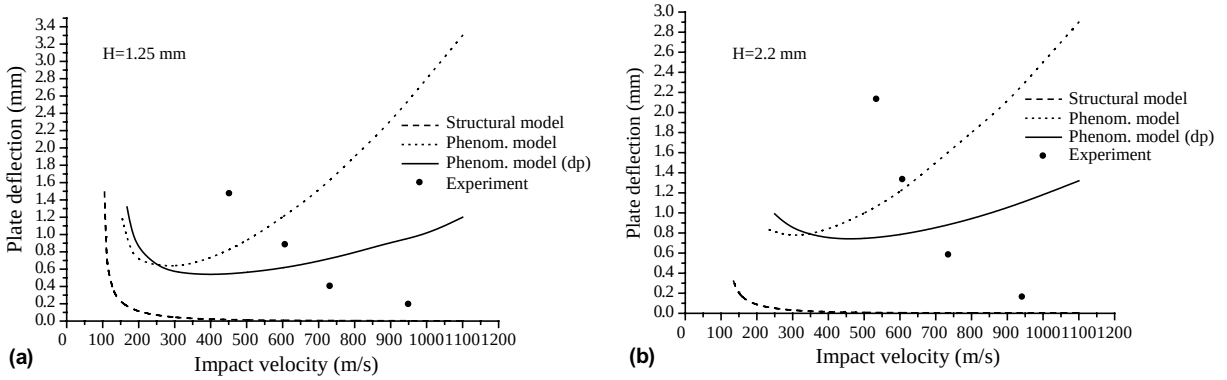

Fig. 9. Deflection of the plate with (a) lower and (b) higher thickness.

Qualitatively, with increasing impact velocity the relative deformation increases, but the computed results are lower than experimental data. Besides, the model gives the same relative deformation for different target thicknesses.

The plug length as a function of impact velocity, for both target thicknesses, is given in Fig. 8 (except for the three-stage model, where this parameter is used as an input value). For both thicknesses, the experimental results are placed between the calculated evaluations from the structural model (that assumes the plug length equal to the plate thickness) and the phenomenological model with a deformable penetrator.

The poorest results, even in a qualitative sense, are obtained for the plate deflection (Fig. 9). The experimental results were expected, because a decrease of plate deflection with increasing impact velocity is the result of a very short duration of the process, i.e. impossibility of spreading and deforming of the secondary zone. In order to correct this discrepancy between the theoretical and experimental results, it is necessary to modify analytical models and take into account all stresses in the secondary target zone (shear, extension and bending), as it was shown by Jenq and Goldsmith (1988).

It is obvious that comparison with experimental results favors the phenomenological model with a deformable penetrator as the most relevant analytical solution of the penetration problem for thin metallic plates.

4. Modified penetration model

In order to obtain better compatibility between theoretical and experimental results, especially for targets of greater thickness, it is necessary to modify the presented phenomenological model with a deformable penetrator. It can be achieved by the correction of the parameter K that takes into account the increase of stress σ in the target material due to the constraint to sideflow provided by the target material surrounding the compressing plug. The original model is very sensitive to the changes of the parameter K. According to Liss et al. (1983) the parameter K represents a material characteristic with constant value $K = [1.7, 2.0]$ during the entire penetration. However, it is clear that the value of parameter K also depends on conditions of compression, particular on the strain ε . This was experimentally verified by Woodward and de Morton (1976). The greater the strain ε and the corresponding stress σ, the greater the parameter of constrained deformation K. As this dependence is not generally known, the modification—as well as in the original model—is referred to the application of the constant, average value of K in the entire process, namely in the first and the second phase when the plug compression occurs. The average values of stress and strain are primarily determined by penetrator impact velocity v_0. So, for a quasi-static compression ($v_0 = 0$) we have the minimum value of considered parameter K_0 and with increasing impact velocity v_0, the stress and strain of the plug material also increase. This causes a gradual increase of K until the impact velocity reaches the velocity of compressive wave in the target material $v_0 = c_p$, where

$$c_p^2 = \frac{1}{\rho}\frac{\partial \sigma_c}{\partial \varepsilon}. \tag{11}$$

When the impact velocity v_0 exceeds the velocity of plastic disturbance c_p, the erosion of the target material occurs and stress obtains the maximum value. This value remains constant with further increase of striking velocity v_0, and therefore the parameter K has also its maximum value K_1. If we assume that K has linear dependence on velocity, it can be written

$$K = \begin{cases} K_0 + \frac{K_1 - K_0}{c_p} v_0, & 0 < v_0 \leqslant c_p, \\ K_1, & c_p \leqslant v_0. \end{cases} \tag{12}$$

where c_p at the initial moment can be calculated from (11), having in mind the constitutive equation for target material (7), as in Liss and Goldsmith (1984):

$$c_p^2 = \lim_{\varepsilon \to 0} \frac{1}{\rho}\frac{\partial \sigma_C}{\partial \varepsilon} = \frac{K_1}{\rho}(\sigma_y + B). \tag{13}$$

The dependence of parameter K on impact velocity is presented in Fig. 10. The values $K_0 = 1.7$ and $K_1 = 3.7$ for the used target material were applied.

The residual velocity as a function of the penetrator impact velocity according to the modified model, which uses Eq. (12) for determination of the parameter K is presented in Fig. 11. A considerably good compatibility between the experimental and computational results of residual velocity is evident for both thinner and thicker plate.

The relative deformation of penetrator diameter remains the same as in the original model (Fig. 7). The plug length and the plate deflection vs. impact velocity are shown in Figs. 12 and 13. The calculated values of plug length follow the experimental results with acceptable accuracy. The highest deviations are still related to the plate deflection, but it can be concluded that the modified model gives significantly better results than the original one.

It is obvious that the modified model improves the correspondence between theoretical and experimental results in the considered case of single, normal penetration of deformable flat-ended projectile into thin metallic targets with ordinance velocities.

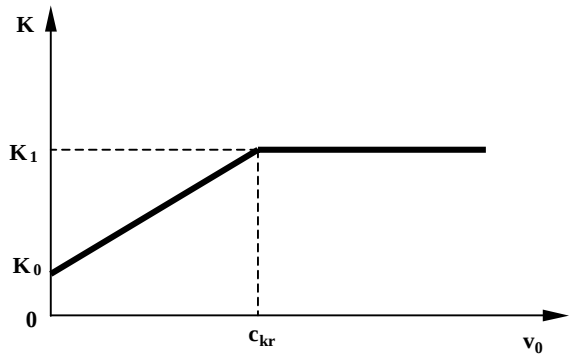

Fig. 10. Dependence of parameter K on penetrator impact velocity.

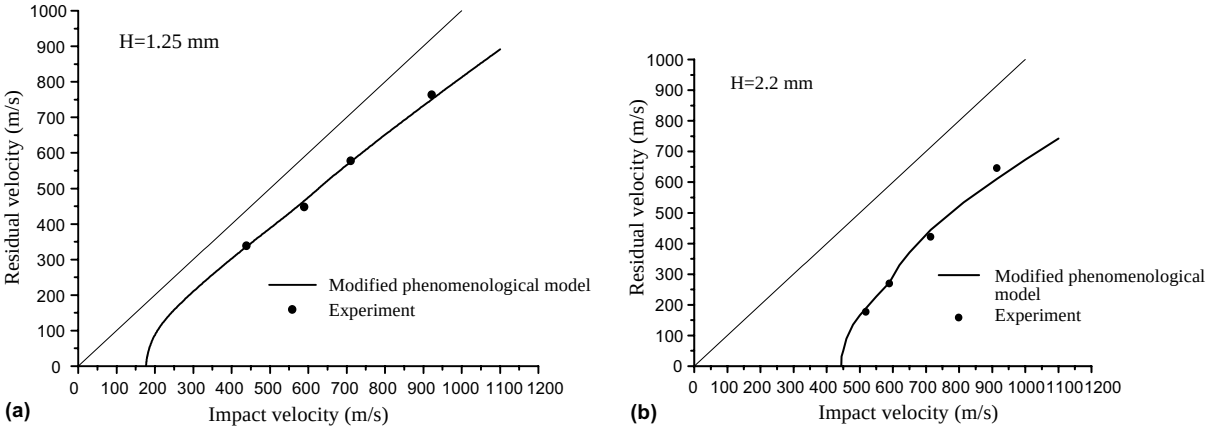

Fig. 11. Penetrator residual velocity vs. impact velocity for the plate with (a) lower and (b) higher thickness (modified model).

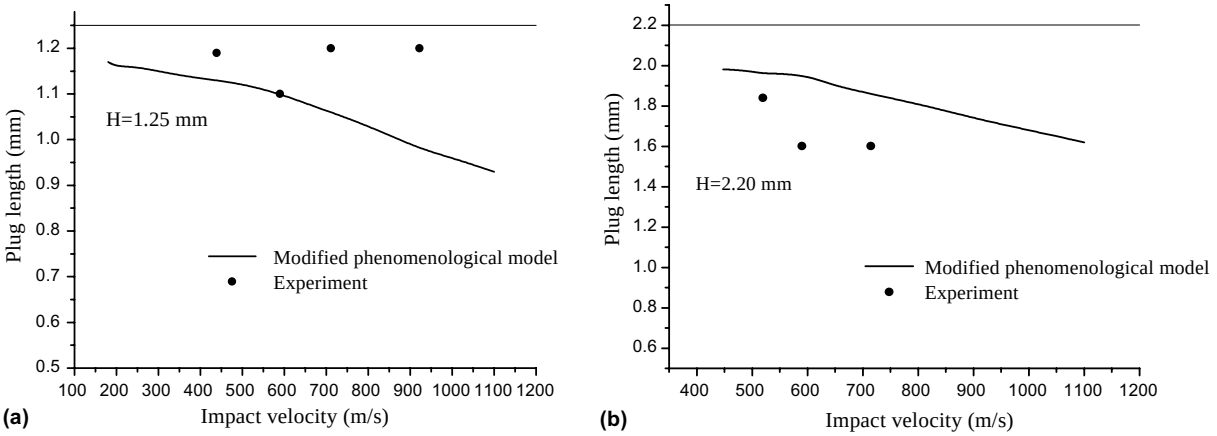

Fig. 12. Plug length vs. penetrator impact velocity for the plate with (a) lower and (b) higher thickness (modified model).

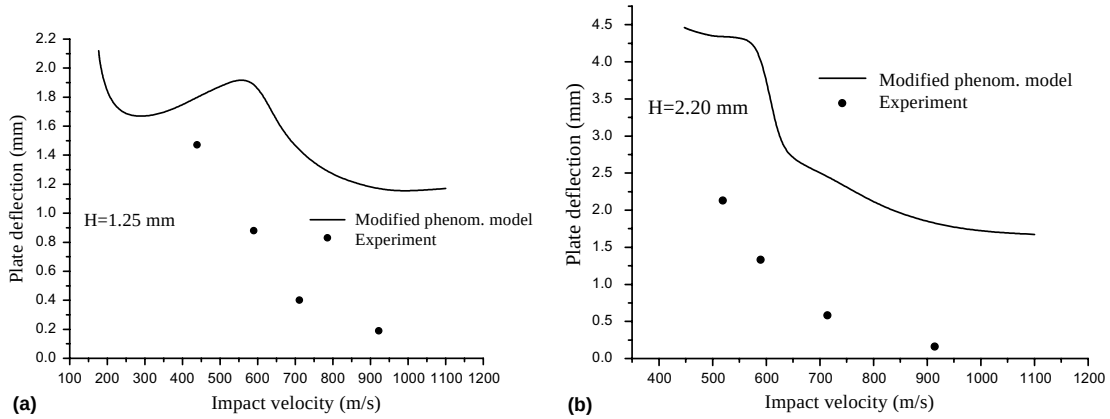

Fig. 13. Plate deflection vs. impact velocity by modified model: (a) plate thickness 1.25 mm, (b) plate thickness 2.20 mm.

5. Perforation of multi-layered target

Modeling of penetration of multi-layered targets is a very complex problem that was considered in numerous papers, e.g. Marom and Bodner (1978) and Radin and Goldsmith (1988). A simplified approach to perforation of multi-layered targets by deformable penetrator, completely based on the application of analytical model for penetration of monolithic targets, will be presented. Considerations are essentially different for the cases of targets with spaced (Fig. 14a) and joined layers (Fig. 14b).

5.1. Perforation of multi-layered target with spaced layers

The perforation of multi-plate target with spaced layers is a significantly simpler problem from the aspect of modeling. By the target with spaced layers, we assume the target where the successive layer has no influence on the current layer perforation. So, the current layer perforation is finished before the effective mass of penetrator (that includes masses of plugs from previous layers) reaches the next layer. If H_i denotes the thickness of ith layer, and L_i the distance between ith and $(i+1)$st layer of the target, it can be conditionally regarded that layers are spaced if it is satisfied

$$L_i \geqslant \sum_{i=1}^{n} H_i, \quad i = \overline{1, n-1}, \tag{14}$$

where n denotes the total number of target layers. This condition is fulfilled if the distance between layers is greater than the length of overall previously formed plug (it is considered that the plug length is approximately equal to the thickness of corresponding layer). Under these conditions the perforation of multi-

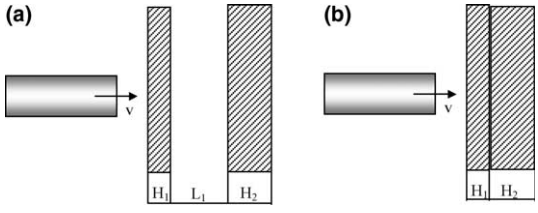

Fig. 14. Cases of penetration of multi-layered targets with (a) spaced and (b) joined layers.

layered target can be regarded as a process that represents simple superposition of penetrations of n single layers. The residual penetrator velocity after the perforation of the current layer is its striking velocity for the successive layer, while the mass of penetrator is increased for the corresponding plug mass. So, it can be written

$$\begin{aligned} &v_{s1} = v_0, \quad (v_r)_i = (v_s)_{i+1}, \\ &m_1 = m, \quad m_{i+1} = m_i + (m_{pl})_i, \quad i = \overline{1, n-1} \end{aligned} \tag{15}$$

where subscript s is related to striking and r to residual velocity of the penetrator. Because the penetrator is deformable, its diameter is assumed to increase after each penetration. So, the diameter of deformed penetrator after the perforation of ith layer $(d_i)_d$ is relevant for the calculation of perforation of the next $(i+1)$st layer

$$d_{i+1} = (d_i)_d, \quad i = \overline{1, n-1}. \tag{16}$$

The given concept, based on conditions (15) and (16), enables the determination of all relevant parameters of the penetration of multi-layered target with the standoff distance between layers, using the model for monolithic target. The flow-chart of computer program is presented in Fig. 15. I and O are vectors of input and output values (velocity, mass and diameter of penetrator), and MODELDEF is the function that performs the calculation of penetration parameters for monolithic target on the basis of the modified phenomenological model with a deformable penetrator.

If target layers are in direct contact ($L_i = 0$), or a standoff distance is lower than L_i defined by (14), we have the case of joined layers that undergoes more complex analysis. Namely, the successive target layer significantly influences the penetration of current layer by increasing resistance to the penetrator progression. It is clear that this influence is manifested by constrained deformation and motion of both primary (plug) and secondary zone of the current layer. So, to treat exactly the phenomena influenced by the next layer, it would probably be necessary to create a completely new analytical model, which is not the subject of this paper. Thus, further analysis is reduced to multiple penetration of spaced layers.

5.2. Analysis of results and discussion

Under the same conditions as for single plates, perforation of double-layered steel joined plates has been performed. Two series of shootings were carried out on the targets formed by different order of plates with 1.25 and 2.20 mm thickness. The average values of measured impact and residual velocities are given in Table 3.

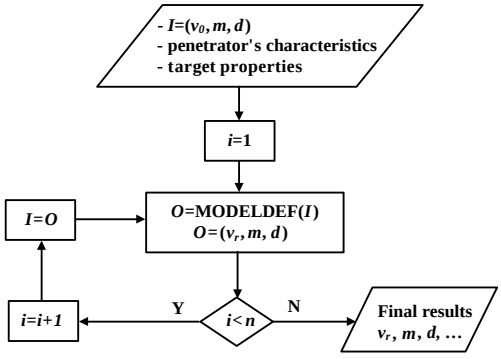

Fig. 15. Flow-chart for determination of penetration parameters for multi-layered target with spaced layers.

The analytical model for penetration of multi-layered targets, based on the simple application of modified phenomenological model, is tested with prior objective so as to determine its qualitative characteristics. Regarding the complexity of investigated phenomena and approximate nature of the model, only the fundamental parameters of penetration process will be considered—the penetrator residual velocity and the ballistic limit velocity (the minimum perforation velocity).

The residual penetrator velocity as a function of its impact velocity is shown in Fig. 16. It should be noted that experimental results were obtained for joined plates and their comparison with theoretical results, based on the model for plates with standoff distance, can be regarded as conditional.

It is shown that the target where the thinner layer (1.25 mm) is in front of the thicker layer (2.20 mm) is more resistant, i.e. obtained residual velocities are lower.

Certainly, the comparison of multi-layered target resistance with equal total thickness (and masses) is both important and interesting. The residual penetrator velocity and the ballistic limit velocity for double-layered plate with standoff distance as a function of relative thickness of the first layer of the target are presented in Fig. 17. Both quantities represent the measures of target resistance—a greater ballistic limit and a lower residual velocity determine a more resistant target. It can be seen from Fig. 17a that the minimum residual velocity is obtained for small thickness of the first layer (impact velocity 919 m/s corresponds to average value of simulator experimental velocities); this velocity gradually increases and reaches the maximum (that defines double-layer target of minimum resistance) when the first layer thickness is 60–80% of the total target thickness. After that, the residual velocity decreases again.

The model provides analogous results for ballistic limit velocity (Fig. 17b). Both diagrams (qualitatively the same for different values of impact velocity and total target thickness) lead to the conclusion that greater resistance of double-layer target is obtained in low thickness of the first layer; the maximum resistance would be obtained in the case of zero thickness of the first layer. This corresponds to the single plate target.

Table 3
Impact and residual velocities in penetration of double-layered target

Thickness of target layers (mm)	Impact velocity (m/s)	Residual velocity (m/s)
1.25 + 2.20	915	405
2.20 + 1.25	923	508

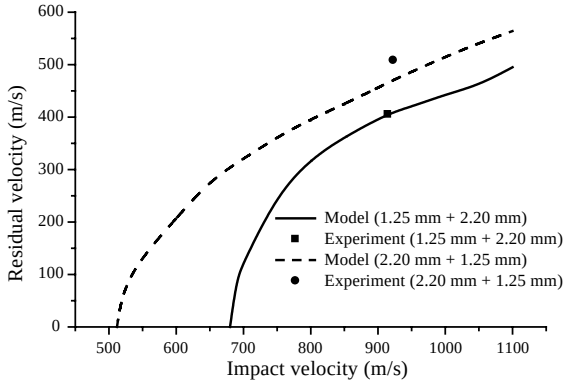

Fig. 16. Residual penetrator velocity vs. impact velocity for double-layered targets. Experimental data are related to joined plates and theoretical results are obtained from the model with spaced layers.

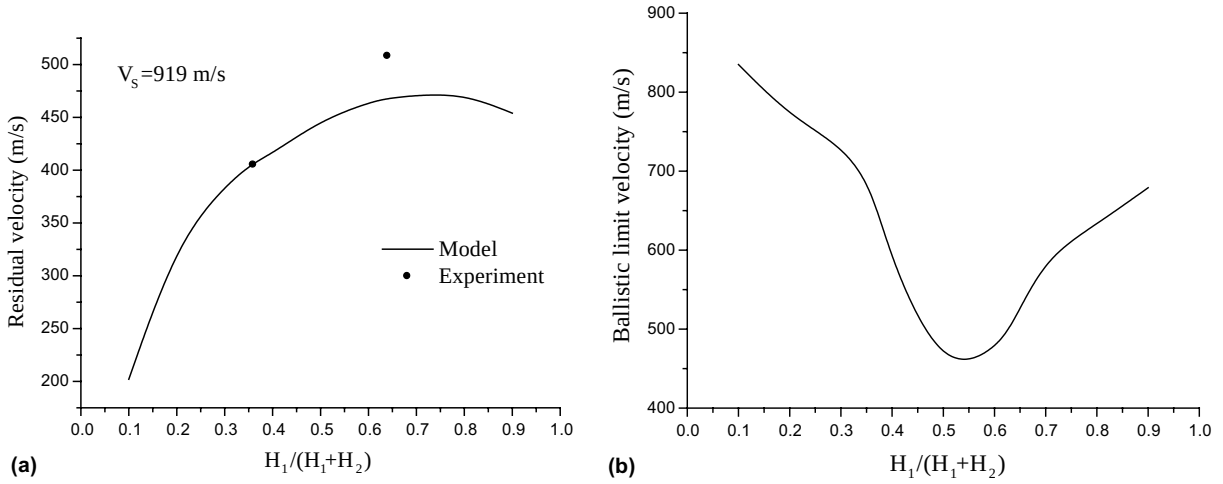

Fig. 17. Influence of relative thickness of the first layer on (a) residual velocity and (b) ballistic limit velocity of double-layered target.

The qualitative explanation of this conclusion is in the fact that during the penetration of monolithic plate the entire structure of target (i.e. secondary zone) resists penetrator progression all the time of penetration and therefore produces greater resistance than individual layers of the multi-layered target. Increase of the first layer share in the total target thickness causes decrease of its resistance. The target resistance reaches minimum at the ratio $H_1/(H_1 + H_2) = 0.5$–0.8. Further increase of the first-layer thickness causes the increase of target resistance again.

Of course, the model provides for consideration of a greater number of layers and their influence on the resistance of multi-layered target. The residual and the ballistic limit velocity as a function of the number of layers n with equal thickness, at constant total mass of the target, are presented in Fig. 18. With increase of the number of layers to $n = 3$ the residual velocity increases, and for triple-layered target and for targets with more than three layers the residual velocity is almost constant. The ballistic limit velocity rapidly drops with increase of the number of layers up to three and then its decrease is gradual. Therefore, the results obtained by applying the analytical model show the fact that increase of the number of layers leads first to rapid and then to moderate decrease of multi-layered target resistance.

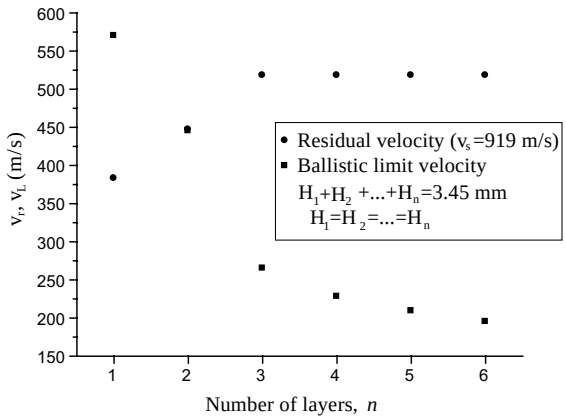

Fig. 18. Influence of number n of spaced layers with equal total mass on penetrator residual velocity and ballistic limit velocity.

All qualitative observations mentioned above are in accordance with published theoretical and experimental results (Nixdorff, 1987); however, they should be proved by independent and more comprehensive experiments.

6. Conclusions

The analysis of perforation of monolithic and multi-layered targets performed on the basis of comparison of our experimental results with the results obtained by analytical models can be reduced to statements as follows:

- The comparison of experimental and model results indicates their good correlation and shows that the phenomenological model with a deformable penetrator seems to be the most adequate analytical approach.
- By correcting the parameter of constraint deformation, the modification of phenomenological model with deformable penetrator has been created; the modification provides qualitatively and quantitatively better results and represents the improvement of the original model.
- The developed analytical model can be adapted for investigating the penetration of multi-layered targets with spaced layers.
- According to the developed model, the monolithic target has greater resistance than any other multi-layered target with standoff distance between layers and equivalent total mass.
- The analysis of double-layered target penetration shows that maximum resistance can be obtained for very low (<20% of total thickness) or very high (>80% of total thickness) first-layer thickness.
- The increase of the number of spaced layers of multi-layered target, at constant total mass, causes further decrease of target resistance.

References

Awerbuch, J., Bodner, S.R., 1974a. Analysis of the mechanics of perforation of projectiles in metallic plates. Int. J. Solids Struct. 10, 671–684.

Awerbuch, J., Bodner, S.R., 1974b. Experimental investigation of normal perforation of projectiles in metallic plates. Int. J. Solids Struct. 10, 685–699.

Jaramaz, S., Micković, D., 2000. Study of penetration of metallic plates using simulators of high-explosive warhead fragments. TR-171/2000, Faculty of Mechanical Engineering, Belgrade.

Jenq, S.T., Goldsmith, W., 1988. Effect of target bending in normal impact of a flat-ended cylindrical projectile near the ballistic limit. Int. J. Solids Struct. 24 (12), 1243–1266.

Liss, J., Goldsmith, W., 1984. Plate perforation phenomena due to normal impact by blunt cylinders. Int. J. Impact Eng. 2 (1), 37–64.

Liss, J., Goldsmith, W., Kelly, J.M., 1983. A phenomenological penetration model of plates. Int. J. Impact Eng. 1 (4), 321–341.

Marom, I., Bodner, S.R., 1978. Projectile perforation of multi-layered beams. Int. J. Mech. Sci. 21, 48–54.

Nixdorff, K., 1987. Discussion of two theories on the penetration of multilayer metallic targets. Trans. CSME 11 (3), 161–178.

Radin, J., Goldsmith, W., 1988. Normal projectile penetration and perforation of layered targets. Int. J. Impact Eng. 7 (2), 229–259.

Woodward, R.L., 1987. A structural model for thin plate perforation by normal impact of blunt projectiles. Int. J. Impact Eng. 6 (2), 129–140.

Woodward, R.L., de Morton, M.E., 1976. Penetration of targets by flat-ended projectiles. Int. J. Mech. Sci. 18, 119–127.